www.sciencemag.org/cgi/content/full/science.aar3958/DC1

Supplementary Materials for

Coactivator condensation at super-enhancers links phase separation and gene control

Benjamin R. Sabari*, Alessandra Dall'Agnese*, Ann Boija, Isaac A. Klein, Eliot L. Coffey, Krishna Shrinivas, Brian J. Abraham, Nancy M. Hannett, Alicia V. Zamudio, John C. Manteiga, Charles H. Li, Yang E. Guo, Daniel S. Day, Jurian Schuijers, Eliza Vasile, Sohail Malik, Denes Hnisz, Tong Ihn Lee, Ibrahim I. Cisse, Robert G. Roeder, Phillip A. Sharp, Arup K. Chakraborty, Richard A. Young†

*These authors contributed equally to this work.
†Corresponding author. Email: young@wi.mit.edu

Published 21 June 2018 on *Science* First Release
DOI: 10.1126/science.aar3958

This PDF file includes:

Other Supplementary Material for this manuscript includes the following:
(available at www.sciencemag.org/cgi/content/full/science.aar3958/DC1)

Materials and Methods

Cell culture

V6.5 murine embryonic stem cells (mESCs) were a gift from the Jaenisch lab. Cells were grown on 0.2% gelatinized (Sigma, G1890) tissue culture plates in 2i media, DMEM-F12 (Life Technologies, 11320082), 0.5X B27 supplement (Life Technologies, 17504044), 0.5X N2 supplement (Life Technologies, 17502048), an extra 0.5mM L-glutamine (Gibco, 25030-081), 0.1mM b-mercaptoethanol (Sigma, M7522), 1% Penicillin Streptomycin (Life Technologies, 15140163), 0.5X nonessential amino acids (Gibco, 11140-050), 1000 U/ml LIF (Chemico, ESG1107), 1μM PD0325901 (Stemgent, 04-0006-10), 3μM CHIR99021 (Stemgent, 04-0004-10). Cells were grown at 37°C with 5% CO_2 in a humidified incubator. For confocal, deconvolution and super-resolution imaging, cells were grown on glass coverslips (Carolina Biological Supply, 633029), glass bottom dishes (Thomas Scientific, 1217N79) or 8-chambered coverglass (Life Technologies, 155409PK or VWR, 100489-104) or glass dishes (Mattek Corporation P35G-1.5-20-C) coated with 5 μg/ml of poly-L-ornithine (Sigma-Aldrich, P4957) for 30 min at 37°C and with 5μg/ml of Laminin (Corning, 354232) for 2hrs-16hrs at 37°C. For passaging, cells were washed in PBS (Life Technologies, AM9625), 1000 U/ml LIF. TrypLE Express Enzyme (Life Technologies, 12604021) was used to detach cells from plates. TrypLE was quenched with FBS/LIF-media, DMEM K/O (Gibco, 10829-018), 1X nonessential amino acids, 1% Penicillin Streptomycin, 2mM L-Glutamine, 0.1mM b-mercaptoethanol and 15% Fetal Bovine Serum, FBS, (Sigma Aldrich, F4135). Cells were spun at 1000rpm for 3 min at RT, resuspended in 2i media and $5x10^6$ cells were plated in 152 cm^2.

HEK293T cells (ATCC, CRL-3216) were used for generation of virus used in optoIDR experiments. HEK293T cells were cultured in DMEM (GIBCO, 11995-073) supplemented with 10% FBS (Sigma Aldrich, F4135), 2mM L-glutamine (Gibco, 25030) and 100 U/mL penicillin-streptomycin (Gibco, 15140), at 37°C with 5% CO_2 in a humidified incubator.

NIH 3T3 cells (ATCC, CRL-3216) were use in optoIDR experiments. NIH 3T3 cells were cultured in DMEM (GIBCO, 11995-073) supplemented with 10% FBS (Sigma Aldrich, F4135), 2mM L-glutamine (Gibco, 25030) and 100 U/mL penicillin-streptomycin (Gibco, 15140), at 37°C with 5% CO_2 in a humidified incubator.

Endogenously-tagged cell line generation

CRISPR/Cas9 was used to generate endogenously-mEGFP-tagged BRD4 and MED1. Oligos coding for guide RNAs targeting the N-terminus of both proteins were cloned into a px330 vector expressing Cas9 and either mCherry (gift from R. Jaenisch) or BFP (Addgene #64323). The sequence that was targeted for BRD4 was 5' TGGGATCACTAGCATGTCTA 3' and the one for MED1 was 5'

TGTCAGGATGAAGGCTCAGG 3'. Repair templates were cloned into a pUC19 vector (NEB) containing mEGFP, a GS linker and 800 bp homology arms flanking the insert. 750K mouse ES were transfected with 1.25 µg px330 vector and 1.25 µg repair templates using lipofectamine. Cells were sorted 2 days after transfection for mCherry and 1 week after first sort for mEGFP. 40K cell were serially diluted in a 6 well plate and colonies were picked 4 days after seeding into a 96 well plate. 2-4 days after colony picking, cells were passaged into 3 plates. 1 plate was used for genotyping and the other 2 were frozen down at -80°C in 10% DMSO, 10% FBS and 80% 1x DMEM. The primer pairs that were used for genotyping were the following:

For BRD4:
5' GCTGTCTTCAGACCCTCCAG 3'
5' GGCATGCACTCTACCACTGA 3'

For MED1:
5' GGTACCCGGGGAGTATCGTCCACTTTGCTA 3'
5' TGCCTGCAGGGGCTGCCCTCATACTCAGAG 3'

Cell treatments

Transfection: cells were transfected with Lipofectamine 3000 (Life Technologies, L3000008) following manufacture's instruction with the following modifications. $1x10^6$ cells in 1ml of FBS/LIF-media were plated in one gelatin-coated well of a 6-multiwell dish and during plating, Lipofectamine-DNA mix was immediately added on top of the cells. After 12hrs, FBS/LIF-media was replaced with 2i media. Cells were imaged 24-48 hrs post transfection.

Nuclei visualization in live cells: cells were treated with Hoechst 33342 for 5min at 37°C in 2i media. Hoechst solution was replaced with fresh 2i media.

1,6-hexanediol treatment for live imaging: cells were grown on glass plates in 1ml of 2i media and cells were imaged every 30s. After the second acquisition, 1ml of 6% 1,6-hexanediol was added on the plate in 10s.

ATP depletion: 2i media was exchanged with glucose free media DMEM (Gibco, 11966025), 0.5X B27 supplement, 0.5X N2 supplement, an extra 0.5mM L-glutamine, 0.1mM b-mercaptoethanol, 1% Penicillin Streptomycin, 0.5X nonessential amino acids, 1000 U/ml LIF, 1µM PD0325901, 3µM CHIR99021) and cultured for 2 hours. 5mM 2-deoxy-glucose (Sigma, D6134) and 126nM Oligomycin (Sigma, 75351) was added and cells were cultured for an additional 2 hours. Cellular ATP levels were measured using a bioluminescence assay (Invitrogen, A22066) following manufacturer's instructions. Control cells were cultured for 4 hours in glucose-containing DMEM (Gibco, 11965-092), 0.5X B27 supplement, 0.5X N2 supplement, an extra 0.5mM L-glutamine, 0.1mM b-mercaptoethanol, 1% Penicillin Streptomycin, 0.5X nonessential amino acids, 1000 U/ml LIF, 1µM PD0325901, 3µM CHIR99021.

Western blot

Cells were lysed in Cell Lytic M (Sigma-Aldrich C2978) with protease inhibitors (Roche, 11697498001). Nuclear lysate was run on a 3%–8% Tris-acetate gel or 10% Bis-Tris gel or 3-8% Bis-Tris gels at 80 V for ~2 hrs, followed by 120 V until dye front reached the end of the gel. Protein was then wet transferred to a 0.45 µm PVDF membrane (Millipore, IPVH00010) in ice-cold transfer buffer (25 mM Tris, 192 mM glycine, 20% methanol) at 300 mA for 2 hours at 4°C. After transfer the membrane was blocked with 5% non-fat milk in TBS for 1 hour at room temperature, shaking. Membrane was then incubated with 1:1,000 anti-BRD4 (Bethyl A301-985A), 1:1,000 anti-MED1 (Abcam ab64965), anti-lamin B1 (Abcam ab16048), anti-RPB1 (Abcam ab817) antibody diluted in 5% non-fat milk in TBST and incubated overnight at 4°C, with shaking. In the morning, the membrane was washed three times with TBST for 5 min at room temperature shaking for each wash. Membrane was incubated with 1:10'000 secondary antibodies for 2 hrs at RT and washed three times in TBST for 5 mins. Membranes were developed with ECL substrate (Thermo Scientific, 34080) and imaged using a CCD camera or exposed using film or with high sensitivity ECL.

Live imaging

Cells were grown on glass plates (Mattek Corporation P35G-1.5-20-C) and before imaging cells culture media was replaced with phenol red-free 2i media and imaged using the Airyscan detector on an LSM880 confocal microscope (Zeiss, Thornwood, NY). Cells were imaged on a heated stage (37°C) and supplemented with warmed (37°C), humidified air. Additionally, microscope was enclosed in an incubation chamber heated to 37°C. ZEN black edition version 2.3 (Zeiss, Thornwood NY) was used for acquisition. Images were acquired with the Airyscan detector in super-resolution (SR) mode with a Plan-Apochromat 63x/1.4 oil objective. Raw Airyscan images were processed using ZEN 2.3 (Zeiss, Thornwood NY).

Immunofluorescence

Immunofluorescence was performed as previously described with some modifications (*70*). Briefly, cells grown on coated glass were fixed in 4% paraformaldehyde, PFA, (VWR, BT140770) in PBS for 10min at RT. After three washes in PBS for 5min, cells were stored at 4°C or processed for immunofluorescence. Cells were permeabilized with 0.5% triton X100 (Sigma Aldrich, X100) in PBS for 5 min at RT. Following three washes in PBS for 5 min, cells were blocked with 4% IgG-free Bovine Serum Albumin, BSA, (VWR, 102643-516) for at least 15min at RT and incubated with primary antibodies (anti-BRD4 Abcam ab128874 1:500 dilution, anti-MED1 Abcam ab64965 1:500 dilution) in 4% IgG-free BSA O/N at RT. After three washes in PBS, primary antibody was recognized by secondary antibodies (Goat anti-Rabbit IgG Alexa Fluor 488 Life Technologies A11008 1:500 dilution, Goat anti-Rabbit

IgG Alexa Fluor 568 Life Technologies A11011 1:500 dilution) in the dark. Cells were washed three times with PBS, 20µm/ml Hoechst 33258 (Life Technologies, H3569) was used to stain nuclei for 5 min at RT in the dark. Glass slides were mounted onto slides with Vectashield (VWR, 101098-042). Coverslips were sealed with transparent nail polish (Electron Microscopy Science Nm, 72180) and stored at 4°C. Images were acquired at the RPI Spinning Disk confocal microscope with 100x objective using MetaMorph acquisition software and a Hammamatsu ORCA-ER CCD camera (W.M. Keck Microscopy Facility, MIT). Images were post-processed using Fiji Is Just ImageJ (FIJI) (*71*) or Imaris v9.0.0 Bitplane Inc. (W.M. Keck Microscopy Facility, MIT), software available at http://bitplane.com.

DNA-FISH combined with immunofluorescence

Immunofluorescence was performed as previously described. After incubating the cells with the secondary antibodies, cells were washed three times in PBS for 5min at RT, fixed with 4% PFA in PBS for 10min and washed three times in PBS. Cells were incubated in 70% ethanol, 85% ethanol and then 100% ethanol for 1min at RT. Probe hybridization mixture was made mixing 7µl of FISH Hybridization Buffer (Agilent G9400A), 1µl of FISH probes and 2µl of water. 5µl of mixture was added on a slide and coverslip was placed on top (cell-side toward the hybridization mixture). Coverslip was sealed using rubber cement. Once rubber cement solidified, genomic DNA and probes were denatured at 78°C for 5 min and slides were incubated at 16C in the dark O/N. Coverslip was removed from slide and incubated in pre-warmed Wash buffer 1 (Agilent, G9401A) at 73°C for 2 min and in Wash Buffer 2 (Agilent, G9402A) for 1 min at RT. Air dry slides and stain nuclei with Hoechst in PBS for 5min at RT. Coverslips were washed three times in PBS, mounted on slide using Vectashield and sealed with nail polish. Images were acquired at the RPI Spinning Disk confocal microscope with 100x objective using MetaMorph acquisition software and a Hammamatsu ORCA-ER CCD camera (W.M. Keck Microscopy Facility, MIT).

DNA FISH probes were custom designed and generated by Agilent to target *Nanog* super enhancer.

Design Input Region – mm9 chr6 122605249 – 122705248
Design Region – mm9 chr6: 122605985-122705394
Coverage 54.56%

RNA-FISH combined with immunofluorescence

Immunofluorescence was performed as previously described with the following modifications. Immunofluorescence was performed in a RNase-free environment, pipettes and bench were treated with RNaseZap (Life Technologies, AM9780). RNase-free PBS was used and antibodies were diluted in RNase-free PBS at all times. After immunofluorescence completion. Cells were post-fixed with 4% PFA in PBS for 10 min at RT. Cells were washed twice with RNase-free PBS. Cells were washed once with 20%

Stellaris RNA FISH Wash Buffer A (Biosearch Technologies, Inc., SMF-WA1-60), 10% Deionized Formamide (EMD Millipore, S4117) in RNase-free water (Life Technologies, AM9932) for 5 min at RT. Cells were hybridized with 90% Stellaris RNA FISH Hybridization Buffer (Biosearch Technologies, SMF-HB1-10), 10% Deionized Formamide, 12.5 μM Stellaris RNA FISH probes designed to hybridize introns of the transcripts of SE-associated genes. Hybridization was performed O/N at 37°C. Cells were then washed with Wash Buffer A for 30 min at 37°C and nuclei were stained with 20μm/ml HOESCH in Wash Buffer A for 5 min at RT. After one 5-min was with Stellaris RNA FISH Wash Buffer B (Biosearch Technologies, SMF-WB1-20) at RT. Coverslips were mounted as described for immunofluorescence. Images were acquired at the RPI Spinning Disk confocal microscope with 100x objective using MetaMorph acquisition software and a Hammamatsu ORCA-ER CCD camera (W.M. Keck Microscopy Facility, MIT).

RNA FISH probes were designed and generated by Biosearch Technologies Stellaris RNA FISH to target introns of *Klf4*, *Nanog*, *Mir290*, *Trim28, Fam168b* and *Zfp606*. Please see Table S3 for the sequences of RNA-FISH probes.

Focus Calling (RNA FISH, DNA FISH, Immunofluorescence)

Foci were called using the "Object Counter3D" plugin in FIJI (https://imagej.nih.gov/ij/plugins/track/objects.html). For each image analyzed, the "Threshold" parameter was set such that punctate bodies in close proximity to one another could be seen as individual objects. For RNA FISH foci of SE-associated genes, the "Min number of voxels" parameter was set to at least 100. For DNA FISH foci the "Min number of voxels" parameter was set to at least 4.

To estimate the number of BRD4 and MED1 foci in live cells, two adjacent nuclear slices were imaged (0.190 μm thickness each, total of 0.38 μm) and BRD4/MEDI foci were called as described above. We divided the number of puncta identified by the volume of the nucleus imaged (area in μm^2 measured with Fiji multiplied by the thickness 0.38 μm) to have an estimate of the number of foci per μm^3. We then multiplied the number of foci per μm^3 by the average volume of nuclei determined by Hoechst staining.

Average image and radial distribution analysis

Custom in-house MATLAB™ scripts were written to process and analyze 3D image data gathered in FISH (RNA/DNA) and IF channels. FISH foci were identified in individual z-stacks through intensity thresholds, centered along a box of size $l = 2.9\ \mu m$, and stitched together in 3-D across z-stacks. The called FISH foci are cross-referenced against a manually curated list of FISH foci to remove false positives, which arise due to extra-nuclear signal or blips. For every DNA or RNA FISH focus identified, signal from the corresponding location in the IF channel is gathered in the l x l square centered at the DNA or RNA FISH focus at every corresponding z-slice. The IF signal centered at FISH

foci for each FISH and IF pair are then combined and an average intensity projection is calculated, providing averaged data for IF signal intensity within a l x l square centered at FISH foci. The same process was carried out for the FISH signal intensity centered on its own coordinates, providing averaged data for FISH signal intensity within a l x l square centered at FISH foci. The number of replicates per average intensity projection is provided for each image set within the text or figure legends. As a control, this same process was carried out for IF signal centered at randomly selected nuclear positions.

Randomly selected nuclear positions were identified for each image set by first identifying nuclear volume and then selecting positions within that volume. Nuclear volumes were determined from DAPI staining through the z-stack image, which was then processed through a custom CellProfiler pipeline (included as auxiliary file). Briefly, this pipeline rescales the image intensity, condenses the image to 20% of original size for speed of processing, enhances detected speckles, filters median signal, Otsu thresholds bodies, removes holes, filters the median signal, dilates the image back to original size, watersheds nuclei, and converts the resulting objects into a black and white image. This black and white image is used as input for a custom R script that uses readTIFF and im (from spatstat (*72*)) to select 40 random nuclear voxels per image set.

These average intensity projections were then used to generate 2D contour maps of the signal intensity or radial distribution plots. Contour plots are generated using in-built functions in MATLAB™. The intensity radial function ($I(r)$) is computed from the average data.

For the contour plots, the intensity-color ranges presented were customized across a linear range of colors ($n_c = 15$). For the FISH channel, black to magenta was used. For the IF channel, we used chroma.js (an online color generator) to generate colors across 15 bins, with the key transition colors chosen as black, blueviolet, mediumblue, lime. This was done to ensure that the reader's eye could more readily detect the contrast in signal. The generated colormap was employed to 15 evenly spaced intensity bins for all IF plots shown in Fig. 1 and Fig S4. The averaged IF centered at FISH or at randomly selected nuclear locations are plotted using the same color scale, set to include the minimum and maximum signal from each plot.

For the radial distribution plots, the spearman correlation coefficients ρ are computed and reported between the FISH and IF (centered at FISH) signal, as well as FISH and the IF (centered at random) signal, for all FISH-IF pairs. A two-tailed student's t-test, comparing the spearman correlation calculated for all pairs, was used to generate p-values.

Fluorescence Recovery After Photobleaching (FRAP)

FRAP was performed on LSM880 Airyscan microscope with 488nm laser. Bleaching was performed over a $r_{bleach} \approx 1um$ using 100% laser power and images were collected every two seconds. Fluorescence intensity was measured using FIJI.

Background intensity was subtracted and values are reported relative to pre-bleaching time points.

Custom MATLAB™ scripts were written to process the intensity data, accounting for background photobleaching and normalization to pre-bleach intensity. Post bleach FRAP recovery data was averaged over 9 replicates for each cell-line and condition. The FRAP recovery curve was fit to:

$$FRAP(t) = M(1 - \exp\left(-\frac{t}{\tau}\right))$$

where FRAP(t) is the normalized FRAP recovery from the average curve. M and τ were inferred through in-built MATLAB functions with 95% confidence intervals. We note that in previous studies (*73, 74*) of typical transcriptional proteins, the role of diffusion on FRAP recovery has been critical. Following (*73*), we estimate an apparent diffusion coefficient:

$$D_{app} = r_{bleach}^2/\tau$$

RNA-Seq analysis

RNA-Seq was performed in untreated mouse embryonic stem cells and used to determine expressed genes. Sequencing reads were aligned to the mm9 revision of the mouse reference genome using Tophat (*75*) with –no-novel-juncs and -G set to a list of known RefSeq transcripts downloaded 2/1/17. Per-transcript expression was quantified as RPKMs using RPKM_count from the RSeQC package (*76*). Expressed transcripts were defined as those with RPKM>1 in at least one of two replicates.

Chromatin immunoprecipitation-sequencing (ChIP-Seq)

mES cells were plated at a density of 0.25 million cells/ml in 2i media and cultured for 24-36 hours. Cells were treated with 2i media with 1.5% 1.6 Hexanediol or 2i media only for 30 minutes. 1% formaldehyde in PBS was used for crosslinking of cells for 10 minutes, followed by quenching with Glycine at a final concentration of 125mM on ice. Cells were washed with cold PBS and harvested by scraping cells in cold PBS. Collected cells were pelleted at 1500 g for 5 minutes at 4°C, resuspended in LB1 (50mM Hepes-KOH, pH7.9, 140mM NaCl, 1mM EDTA 0.5mL 0.5M, 10% glycerol, 0.5% NP40, 1% TritonX-100, 1x protease inhibitor) and incubate for 20 minutes rotating at 4°C. Cells were pelleted for 5 minutes at 1350 g, resuspended in LB2 (10 mM Tris pH 8.0, 200 mM NaCl, 1 mM EDTA, 0.5 mM EGTA, 1x protease inhibitor) and incubated for 5 minutes rotating at 4°C. Pellet was resuspended in LB3 (10 mM Tris pH 8.0, 100 mM NaCl, 1 mM EDTA, 0.5 mM EGTA, 0.1% sodium-deoxycholate, 0.5% sodium lauroyl sarcosinate, 1% TritonX-100, 1x protease inhibitor) at a concentration of 30-50 million cells/ml. Cells were sonicated using Covaris S220 for 12 minutes using the manufacturer's instructions followed by spinning at 20 000g for 30 minutes at 4°C. Dynabeads pre-blocked with 0.5% BSA were incubated with Brd4 A301-985A Bethyl, Med1 A300-793A-4 Bethyl or Pol II 8WG16 (Abcam ab817) antibody for 2 hours. Chromatin was added to antibody-bead complex and incubated rotating overnight at 4°C.

Beads were washed three times with each Wash buffer 1 (50mM Hepes pH7.5, 500mM NaCl, 1mM EDTA, 1mM EGTA,1% Triton, 0.1% NaDoc, 0.1% SDS) and Wash Buffer 2 (20mM Tris pH 8, 1mM EDTA, 250mM LiCl, 0.5% NP40, 0.5% NaDoc) at 4°C, followed by washing one time with TE at room temperature. Chromatin was eluted by adding Elution buffer (50 mM, Tris pH 8.0, 10 mM EDTA, 1% sodium dodecyl sulfate, 20ug/ml RNaseA) to the beads and incubated shaking at 60°C for 30 minutes. Reversal of crosslinking was performed for 4 hours at 58°C. Proteinase K was added and incubated for 1-2 hours at 37°C for protein removal. DNA was purified using Qiagen PCR purification kit and resuspended in 10mM Tris-HCL.

ChIP Libraries were prepared with the Swift Biosciences Accel-NGS® 2S Plus DNA Library Kit according to kit instructions with an additional size selection step on the PippinHT system from Sage Science. Following library prep, ChIP libraries were run on a 2% gel on the PippinHT with a size collection window of 200-600 bases. Final libraries were quantified by qPCR with the KAPA Library Quantification kit from Roche and sequenced in single-read mode for 40 bases on an Illumina HiSeq 2500.

ChIP-Seq analysis

ChIP-Seq data were aligned to the mm9 version of the mouse reference genome using bowtie with parameters –k 1 –m 1 –best and –l set to read length. Wiggle files for display of read coverage in bins were created using MACS (*77*) with parameters –w –S –space=50 –nomodel –shiftsize=200, and read counts per bin were normalized to the millions of mapped reads used to make the wiggle file (*78*). Reads-per-million-normalized wiggle files were displayed in the UCSC genome browser (*79*).

Super-enhancer identification

Super-enhancers were identified as described in Whyte et al. with minor modifications *(14)*. Peaks of enrichment in MED1 were identified using MACS with –p 1e-9 –keep-dup=1 and input control. MED1 aligned reads from the untreated condition and corresponding peaks of MED1 were used as input for ROSE (https://bitbucket.org/young_computation/) with parameters -s 12500 -t 2000 -g mm9 and input control. A custom gene list was created by adding D7Ertd143e, and removing Mir290, Mir291a, Mir291b, Mir292, Mir293, Mir294, and Mir295 to prevent these nearby microRNAs that are part of the same transcript from being multiply counted. Stitched enhancers (super-enhancers and typical enhancers) were assigned to the single expressed RefSeq transcript whose promoter was nearest the center of the stitched enhancer. Expressed transcripts were defined as above. Super-enhancers and typical enhancers identified in this approach and their assigned genes are included as Supplemental Table S2.

ChIP-Seq signal after 1,6-hexanediol treatment

Log2 fold-changes of BRD4, MED1, or RNAPII ChIP-Seq signal were calculated by determining coverage of super-enhancers, typical enhancers, or gene bodies (transcription start site to transcription end site) using bedtools intersect (*80*). PCR duplicates were removed using samtools rmdup (*81*) and used as input. Read counts were normalized to the millions of mapped, duplicate-removed reads. Both ChIP and input control samples were analyzed similarly, and the input control values were subtracted in corresponding regions in corresponding treatments. A pseudocount of 1 was added to the RPM-normalized, background-subtracted values in each treatment, and a log2 fold-change was calculated and plotted. Per-super-enhancer fold-changes in RPM-normalized, background-subtracted values of BRD4 and MED1 are compared with a Spearman correlation coefficient.

Sequence data has been uploaded to GEO under the following accession number: GSE112808

Gene Set Enrichment Analysis

RefSeq genes were ranked by their loss of RNAPII signal upon 1,6-hexanediol treatment and used as input for GSEA pre-ranked (*82*). Super-enhancer associated genes were used as the gene set.

Comparing BRD4 and MED1 ChIP-Seq colocalization

To compare BRD4 and MED1 colocalization on the genome, we analyzed read counts of untreated BRD4 and MED1 ChIP-Seq in 10000 bp bins that tile the genome. Non-PCR-duplicate reads were quantified in 10000 bp bins using bedtools intersect. Bins were subsetted for those that overlapped super-enhancers by at least 1 bp using bedtools intersect.

ChIA-PET analysis

For each ChIA-PET dataset, raw reads were processed to identify a set of putative interactions that connect interaction anchors for further statistical modeling and analysis. First, paired-end tags (PETs), each containing two paired reads, were analyzed for the presence of the bridge-linker sequence and trimmed to facilitate read mapping. PETs containing at least one instance of the bridge-linker sequence in either of the two reads were kept for further processing and reads containing the bridge-linker sequence were trimmed immediately before the linker sequence using cutadapt with options

‘‘-n 3 O 3 -m 15 -a forward=ACGCGATATCTTATCTGACT -a reverse=AGTCAGATAAGATATCGCGT’’ (http://cutadapt.readthedocs.io/en/stable/). PETs that did not contain an instance of the bridge-linker sequence were not processed further. Trimmed reads were mapped individually to the mm9 mouse reference genome using Bowtie with options ‘‘-n 1 -m 1 -p 6’’(*77*). After alignment, paired reads were re-linked with an in-house script using read identifiers. To avoid potential artifacts arising

from PCR bias, redundant PETs with identical genomic mapping coordinates and strand information were collapsed into a single PET. Potential interaction anchors were determined by identifying regions of local enrichment in the individually mapped reads using MACS with options ‘‘-g mm -p 1e-9–nolambda–nomodel–shiftsize=100’’(*78*). PETs with two mapped reads that each overlapped a different potential interaction anchor by at least 1 bp were used to identify putative interactions between the overlapped interaction anchors. Each putative interaction represents a connection between two interaction anchors and is supported by the number of PETs (PET count) that connect the two interaction anchors.

Protein purification

cDNA encoding the BRD4-IDR or MED1-IDR were cloned into a modified version of a T7 pET expression vector. The base vector was engineered to include a 5’ 6xHIS followed by either mEGFP or mCherry and a 14 amino acid linker sequence “GAPGSAGSAAGGSG.” NEBuilder® HiFi DNA Assembly Master Mix (NEB E2621S) was used to insert BRD4-IDR or MED1-IDR sequence (generated by PCR) in-frame with the linker sequence. Vectors expression mEGFP alone contain the linker sequence followed by a STOP codon. The MED1-IDR_S-to-A mutant was synthesized as a geneblock (IDT) and was inserted into the same base vector as described above. All expression constructs were sequenced to ensure sequence identity.

Plasmids containing the protein of interest fused to mEGFP or mCherry were transformed into LOBSTR cells (gift of Chessman Lab). A fresh bacterial colony was inoculated into LB media containing kanamycin and chloramphenicol and grown overnight at 37^{o}C.

Cells containing the BRD4-IDR construct were diluted 1:30 in 500ml room temperature LB with freshly added kanamycin and chloramphenicol and grown 1.5 hours at 16^{o}C. IPTG was added to 1mM and growth continued for 18 hours. Cells were collected and stored frozen at -80^{o}C. Cell containing all other constructs were treated in a similar manner except they were grown at 37 ^{o}C for 1.5 hours prior to IPTG addition and then for 5 hours at 37 ^{o}C after addition of IPTG. Cells were collected and stored frozen at -80^{o}C.

Pellets from 500ml cells were resuspended in 15ml of Buffer A (50mM Tris pH7.5, 500 mM NaCl) containing 10mM imidazole, cOmplete protease inhibitors (Roche, 11873580001) and sonicated (ten cycles of 15 seconds on, 60 sec off). The lysate was cleared by centrifugation at 12,000g for 30 minutes at 4^{o}C and added to 1ml of Ni-NTA agarose (Invitrogen, R901-15) pre-equilibrated with 10X volumes of buffer A. Tubes containing this agarose lysate slurry were rotated at 4^{o}C for 1.5 hours. The slurry was poured into a column, and the packed agarose washed with 15 volumes of Buffer A containing 10mM imidazole. Protein was eluted with 2 X 2ml Buffer A containing 50mM imidazole, 2 X 2ml Buffer A with 100mM imidazole, followed by 4 X 2ml Buffer A with 250mM imidazole.

Elutions containing protein as judged by coomassie stained gel were combined and dialyzed against Buffer D (50mM Tris-HCl pH 7.5, 500mM NaCl, 10% glycerol, 1mM DTT).

In vitro droplet assay

Recombinant mEGFP fusion proteins were concentrated and desalted to an appropriate protein concentration and 125mM NaCl using Amicon Ultra centrifugal filters (30K MWCO, Millipore). Recombinant protein was added to solutions at varying concentrations with indicated final salt and molecular crowder concentrations in Buffer D (50mM Tris-HCl pH 7.5, 10% glycerol, 1mM DTT). The protein solution was immediately loaded onto a homemade chamber comprising a glass slide with a coverslip attached by two parallel strips of double-sided tape. Slides were then imaged with an Andor confocal microscope with a 100x objective. Unless indicated, images presented are of droplets settled on the glass coverslip.

For droplet assay within the in vitro transcription reaction, activator (HNF4α, 100 ng per reaction), template ($pA_{4x}ML\Delta 53$, 50 ng per reaction), and HeLa cell nuclear extract (3mg/ml, final concentration) were incubated with mEGFP or mEGFP fusion proteins with wild-type or mutant MED1-IDR at the indicated concentrations, followed by imaging as described above.

For experiments with fluorescently labeled dextrans, droplets were formed with indicated concentration of protein in Buffer D with 125mM NaCl and 10% Ficoll-400, followed by addition of TRITC-labeled dextrans with average molecular weights of 4,400 (Sigma T1037), 10,000 (Invitrogen D1816), or 40,000 (Invitrogen D1842). Dextrans and droplets were allowed to mix for 5 minutes at room temperature followed by imaging as described above.

OptoIDR assay

The optoIDR assay was adapted from Shin, Y et al Cell 2017 *(44)*. For cloning of IDRs, DNA segments encoding intrinsically disordered domains were amplified using Phusion Flash (Thermo Fisher F548S). Segments were cloned into generation II lentiviral backbone containing the mCherry-Cry2 fusion protein (obtained from the Brangwynne laboratory) using Hi-Fi NEBuilder (NEB E2621S). Cloned opto-droplet plasmids were co-transfected with psPAX (Addgene 12260), and pMD2.G (Addgene 12259) viral packaging plasmids using PEI transfection reagent (polysciences 23966-1).Virus was produced in HEK293T cells, and was either used directly or concentrated using Takara Lenti-X Concentrator (631232). For transductions, 3T3 Cells were plated 1 day prior to transduction, seeded at 400,000 cells per 35mm tissue culture well. Viral media was added to cells for 24 hours, at which point cells were expanded in normal media for either imaging or propagation. For imaging, 35mm MatTek glass-bottom dishes (MatTek P35G-1.5-20-C) were coated for with 0.1mg/ml fibronectin (EMD-Millipore FC010) for 20 minutes at 37°C and washed twice with PBS prior to plating. Cells were plated at

400,000 cells per 35mm dish one day before imaging. Imaging was performed on Zeiss LSM 710 point scanning microscope. Unless otherwise indicated, droplet formation was induced with 488nm light pulses every 2 seconds for the duration of imaging, with images also taken every 2 seconds. Duration of imaging as indicated. mCherry fluorescence was stimulated with 561nm light. For FRAP experiments, droplet formation was induced with 488nm light for 40 seconds, at which point foci were bleached with 561nm light and recovery was imaged every 2 seconds in the absence of 488nm stimulation.

In vitro transcription

In vitro transcription reactions (25 μl) were assembled as previously described *(69)* with slight modifications. Briefly, the activator (HNF4α, 100 ng per reaction) was pre-incubated with the template ($pA_{4x}MLΔ53$, 50 ng per reaction) on ice for 10 min. mEGFP or mEGFP fusion proteins with wild-type or mutant MED1-IDR at the indicated concentration and HeLa cell nuclear extract were then added (final concentration of 3mg/ml). Following a 40 min incubation at $30^{O}C$, a nucleotide triphosphate mix formulated for G-free templates and containing [α-^{32}P]CTP was added and transcription was allowed to take place for 30 min at $30^{O}C$. Reactions were stopped, processed for electrophoresis on 5% denaturing polyacrylamide gels and visualized by autoradiography as described *(69)*.

Droplet pelleting

Activator (HNF4α, 100 ng per reaction), template ($pA_{4x}MLΔ53$, 50 ng per reaction), and HeLa cell nuclear extract (final concentration 3mg/ml) were incubated with mEGFP or mEGFP fusion proteins with wild-type or mutant MED1-IDR at the indicated concentrations for 10 minutes at room temperature. For immunoblots of pelleted fractions, solutions were centrifuged at 10,000xg for 10 minutes. Sups were removed and pellets were resuspended in XT sample buffer (Biorad).

Constructs

	Source
mCherry-Cry2WT	Brangwynne laboratory
pET-mEGFP-BRD4-IDR	This manuscript
pET-mEGFP-MED1-IDR	This manuscript
pET-mEGFP	This manuscript
pET-mCherry-MED1-IDR	This manuscript
pET-mEGFP-MED1-IDR_S-to-A	This manuscript
OptoIDR-MED1-frag1	This manuscript

Fig S1

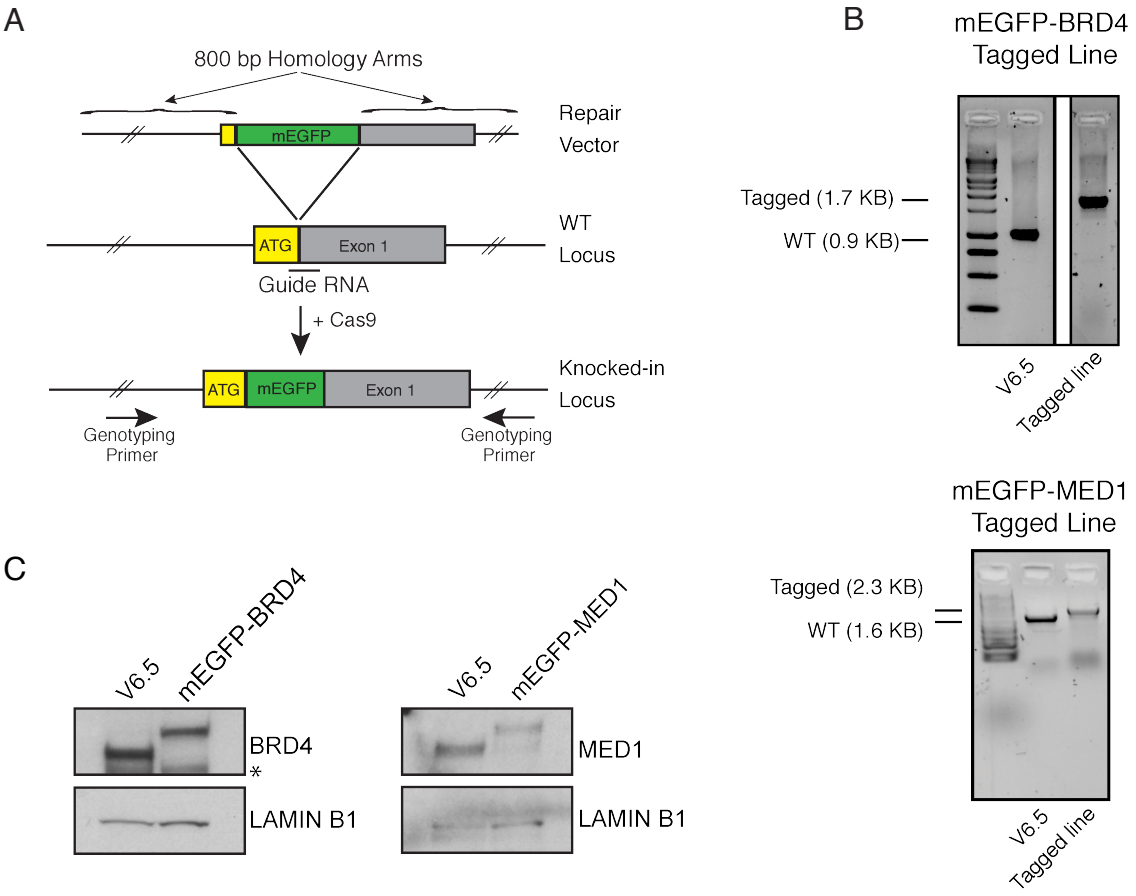

Fig. S1. Generation and validation of endogenously tagged mEGFP-BRD4 and mEGFP-MED1 mESC lines.

(**A**) Schematic of knock-in strategy. V6.5 mouse embryonic stem cells (parental line) were transfected with a plasmid expressing Cas9, guide, and a repair vector with 800bp homology arms. 20bp guide RNAs were designed to span the insertion site (start codon) adjacent to a PAM sequence (NGG). (**B**) Agarose gel of genotyping PCR for clonal lines of mEGFP-BRD4 (top) and mEGFP-MED1 (bottom). (**C**) Immunoblot validation of endogenous levels of expression for mEGFP-BRD4 and mEGFP-MED1 cell lines. Cell lysates from parental mESCs (V6.5) and the indicated engineered cell line were subject to immunoblots with the indicated antibodies. The shift in molecular weight is of the size expected for mEGFP fusion. The asterisk designates a non-specific band in the BRD4 immunoblot.

Fig. S2

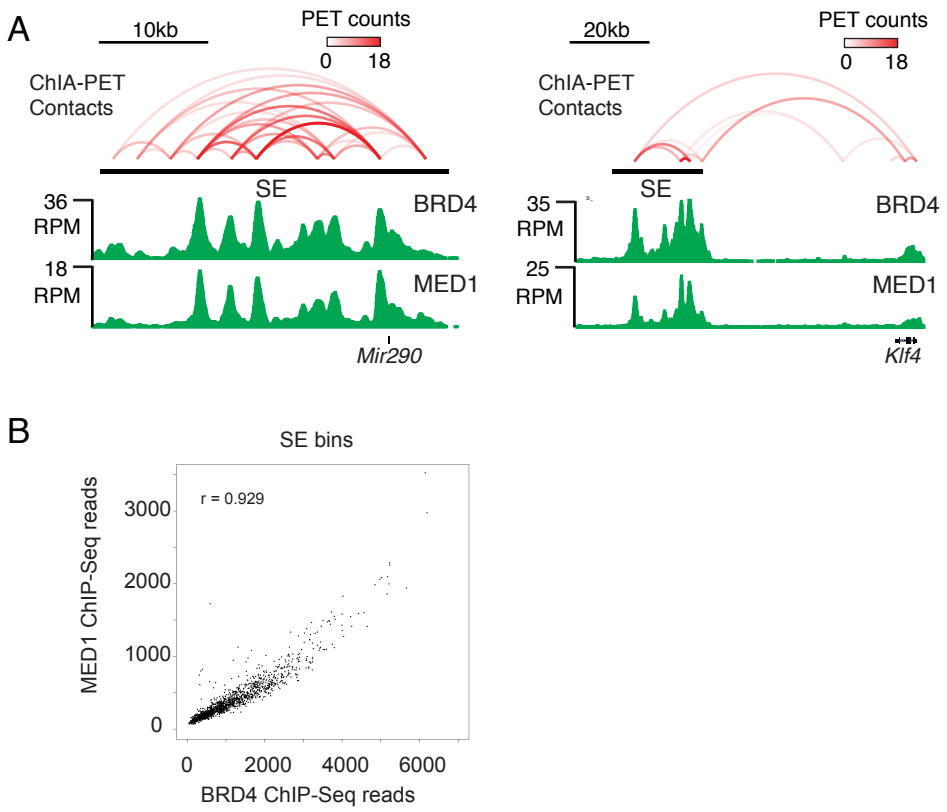

Fig. S2. Super-enhancer constituents are occupied by both BRD4 and MED1 and are in close spatial proximity.

(**A**) Genome browser view of SMC1A ChIA-PET data indicating the regions with high contact frequency and BRD4 and MED1 ChIP-seq at the *Mir290* and *Klf4* loci. (**B**) Scatter plot representation of ChIP-seq reads per million mapped reads (rpm) within 10kb bins tiled over the genome that contain super-enhancers (SE bins) for MED1 versus BRD4. Spearman correlation r-value is presented.

Fig. S3

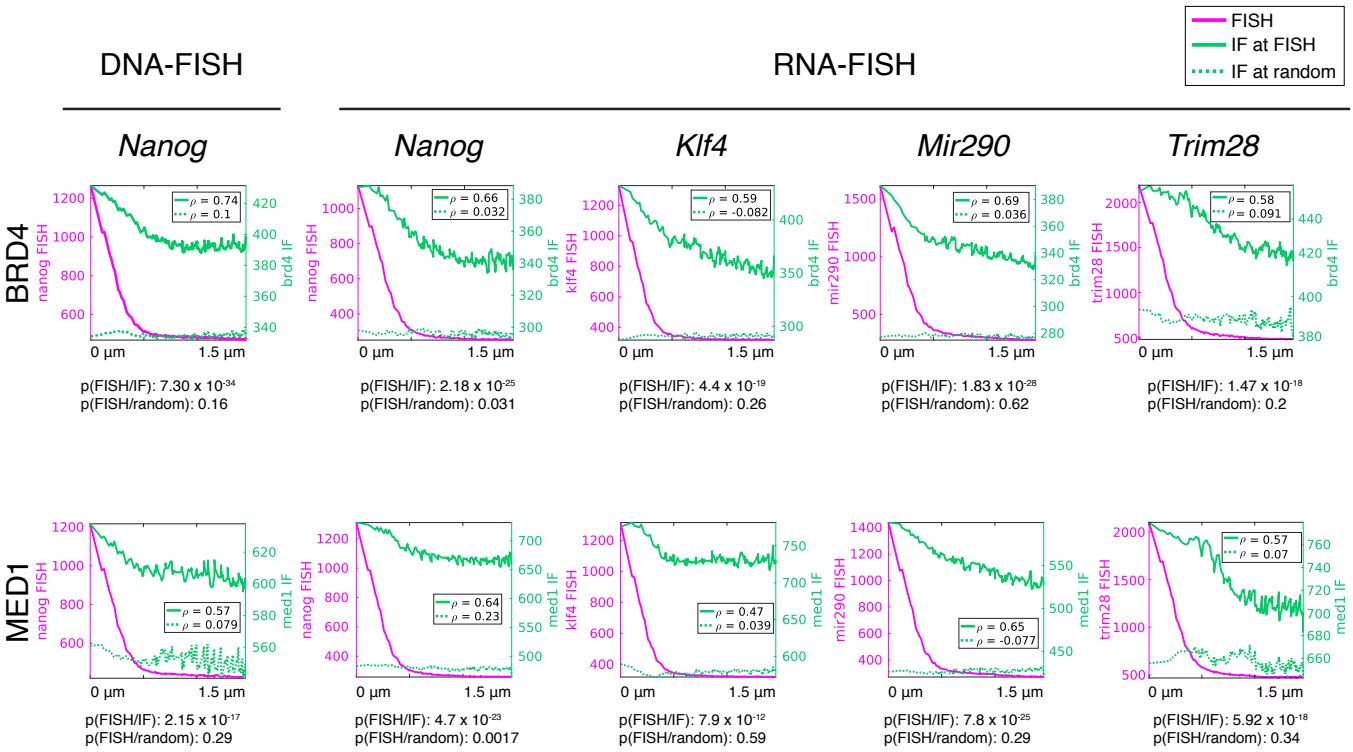

Fig. S3. Radial distribution analysis of the average IF images centered at FISH foci

Radial distribution functions of averaged IF images centered at indicated DNA-FISH, RNA-FISH, or randomly selected nuclear position (random). The far left panel shows information for DNA-FISH for the *Nanog* locus combined with IF for BRD4 or MED1. The radial distribution of averaged fluorescence intensity as a function of distance from the center of FISH foci is shown for FISH signal (magenta) and BRD4 or MED1 signal (green) or of averaged fluorescence intensity of BRD4 or MED1 as a function of distance from the center of randomly selected nuclear location (dashed green). Spearman correlation analysis comparing the radial distributions of average FISH at FISH foci (FISH, magenta) to average IF at FISH foci (IF at FISH, green) or to average IF at randomly selected nuclear locations (IF at random, dashed green) were performed, Spearman coefficient (ρ) and the p-value of a two-tailed student's t-test are presented for each comparison. The remaining panels show radial distribution functions and statistics for RNA-FISH probing *Nanog*, *Klf4, Mir290 or Trim28* combined with IF for BRD4 or MED1, as described for DNA-FISH. Nascent RNA FISH probes designated "*Mir290*" are designed to probe the precursor RNA which codes for the cluster of microRNAs *Mir290-295*.

Fig. S4

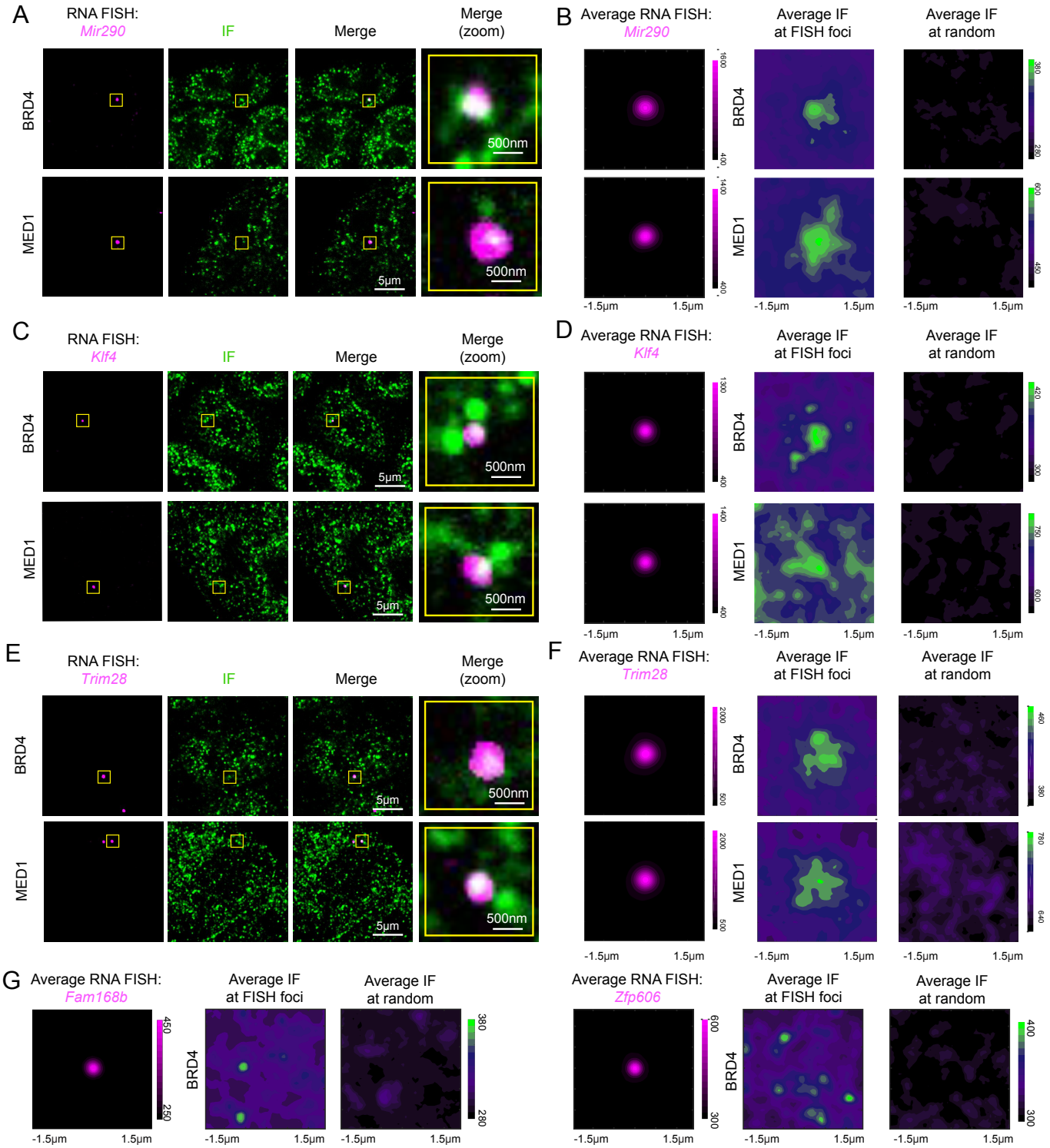

Fig. S4. Extended analysis of IF and nascent RNA FISH

(**A**) Representative images of co-localization between BRD4 or MED1 and the nascent RNA of SE-associated gene *Mir290* by IF and FISH in mESC. Samples were imaged using spinning disk confocal microscopy. A single z-slice is presented. Co-localization region highlighted in a yellow box is blown-up in the "Merge (zoom)" column. (**B**) Average fluorescence centered at either *Mir290* RNA-FISH foci (N = 212 for BRD4, N = 290 for MED1) or randomly selected nuclear position with +/- 1.5 microns in X and Y. Color scale bars present arbitrary units of fluorescence intensity. (**C**) same as (A) for SE-associated gene *Klf4*. (**D**) Same as (B) for *Klf4* (N = 58 for BRD4, N = 127 for MED1). (**E**) same as (A) for SE-associated gene *Trim28*. (**F**) Same as (B) for *Trim28* (N = 271 for BRD4, N = 230 for MED1). (**G**) BRD4 puncta do not overlap with *Fam168b* or *Zfp606* RNA-FISH foci. Same as (B) for either *Fam168b* RNA-FISH foci (N =111) (left) or *Zfp606* (N = 50) (right).

Fig. S5

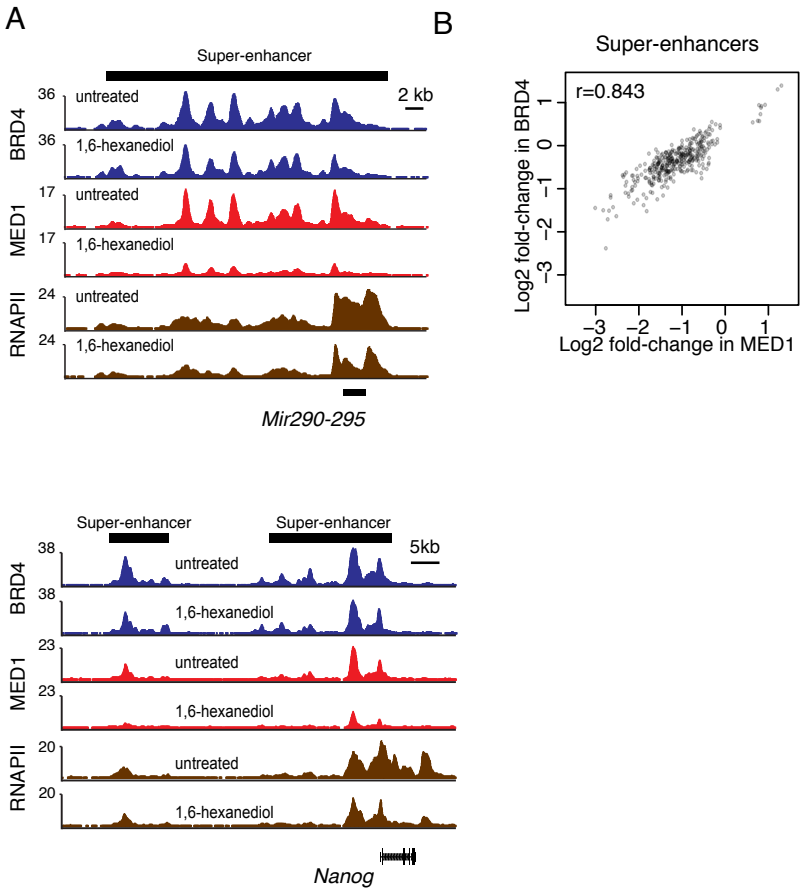

Fig. S5. 1,6-hexanediol treatment leads to a loss of BRD4, MED1, and RNAPII preferentially at super-enhancers

(**A**) Genome browser view of BRD4, MED1, and RNAPII ChIP-seq data in untreated and 1,6-hexanediol treated cells (1.5%, 30 minutes) at the super-enhancers associated with either *Mir290-295* (top) or *Klf4* (bottom). (**B**) Correlation between the loss of BRD4 or MED1 at super-enhancers. Scatterplot representation of all super-enhancers plotted as log2(fold-change) of BRD4 by log2(fold-change) of MED1.

Fig. S6

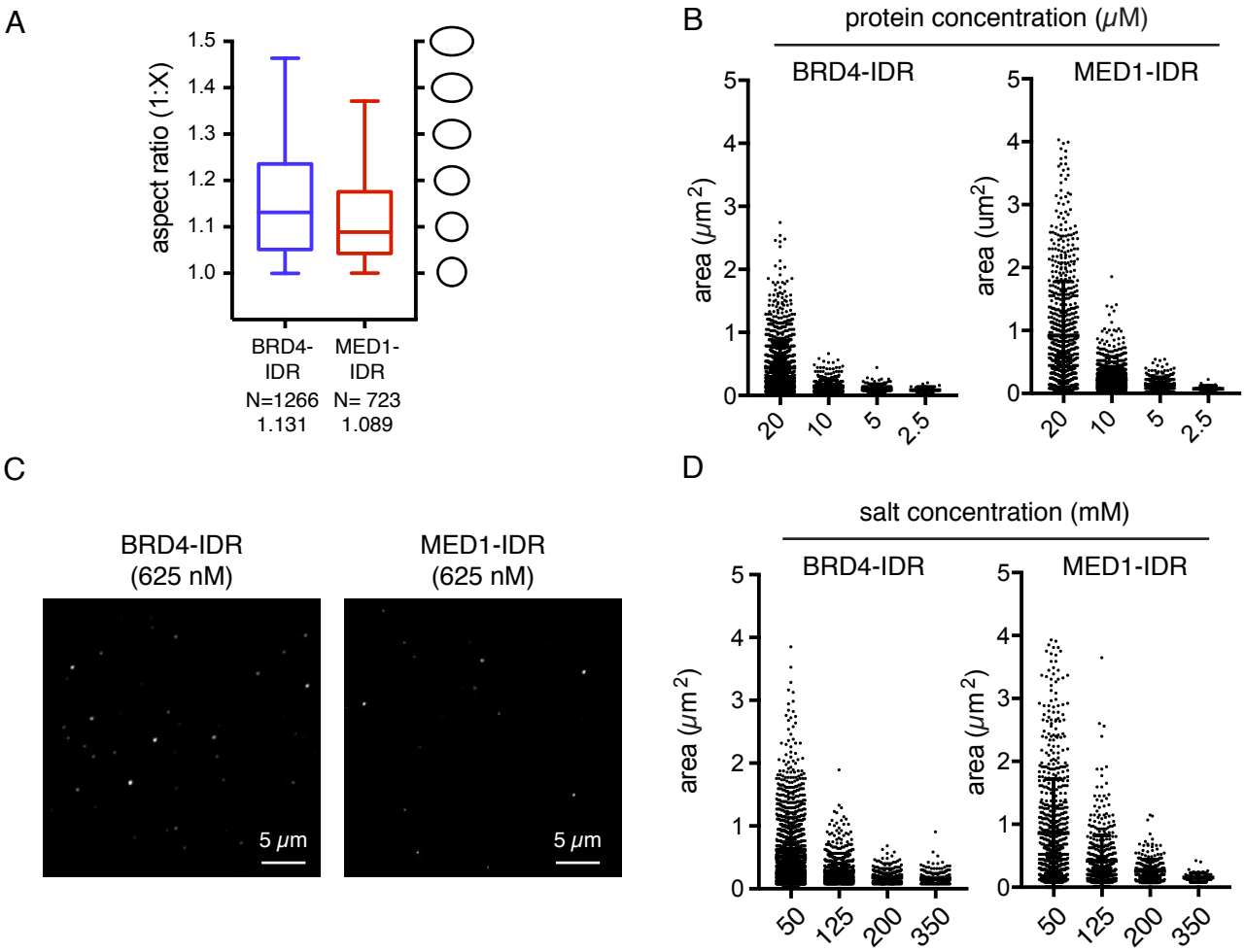

Fig. S6. Extended analysis of MED1-IDR and BRD4-IDR droplets

(**A**) Box plots showing the distribution of aspect ratios for droplets of BRD4-IDR and MED1-IDR. The numbers of droplets examined and the mean aspect ratios are shown. Box plot represents 10-90th percentile. (**B**) Dot plot showing the relationship between protein concentration and droplet size for BRD4-IDR (left panel) or MED1-IDR (right panel). Protein concentration (μM) is shown on the x-axis and droplet size as a function of area in a 2-D image is shown on the y-axis. (**C**) Image showing the presence of small droplets at low protein concentrations. (**D**) Dot plot showing relationship between salt concentration and droplet size for BRD4-IDR (left panel) or MED1-IDR (right panel). Salt concentration (mM) is shown on the x-axis and droplet size as a function of area in a 2-D image is shown on the y-axis.

Fig. S7

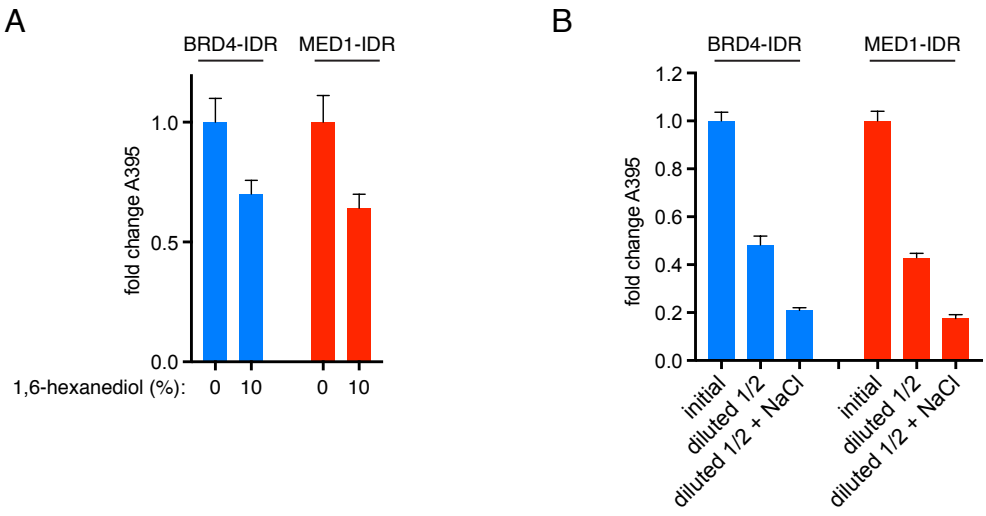

Fig. S7. Densitometry analysis of BRD4-IDR and MED1-IDR droplets under various conditions (**A**) Normalized densitometry upon incubation with 10% 1,6-hexanediol. Absorbance measurements at 395nm (A395) were taken for BRD4-IDR or MED1-IDR droplets (10μM protein, 125mM NaCl) with or without 10% hexanediol in the presence of 10% PEG-8000. Absorbance measures were normalized to untreated samples. Data are presented as averages +/- SD of three independent experiments measured in technical triplicate. (**B**) Normalized densitometry in reversibility assay. Absorbance measurements at 395nm (A395) were taken for droplets formed of either BRD4-IDR or MED1-IDR, as indicated, (20 μM protein, 75 mM NaCl) (initial) or followed by a 1:1 dilution (diluted 1/2) or a 1:1 dilution with an increase to 425mM NaCl (diluted 1/2 + NaCl), in presence of 10% PEG-8000. Data are presented as averages +/- SD of three independent experiments measured in technical triplicate.

Fig. S8

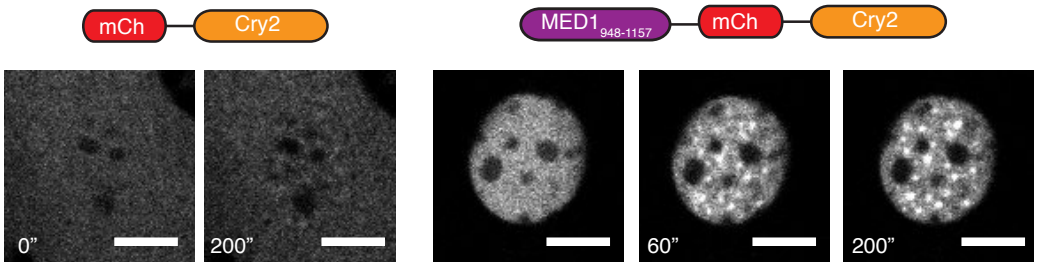

Fig. S8. Blowup of individual nucleus under blue light-stimulation
Zoom in on the nucleus of cells expressing either mCherry-Cry2 or MED1-IDR-mCherry-Cry2 after the indicated duration of blue light stimulation, selected from Fig. 5B and 5C. Scale bar, 10μm

Fig. S9

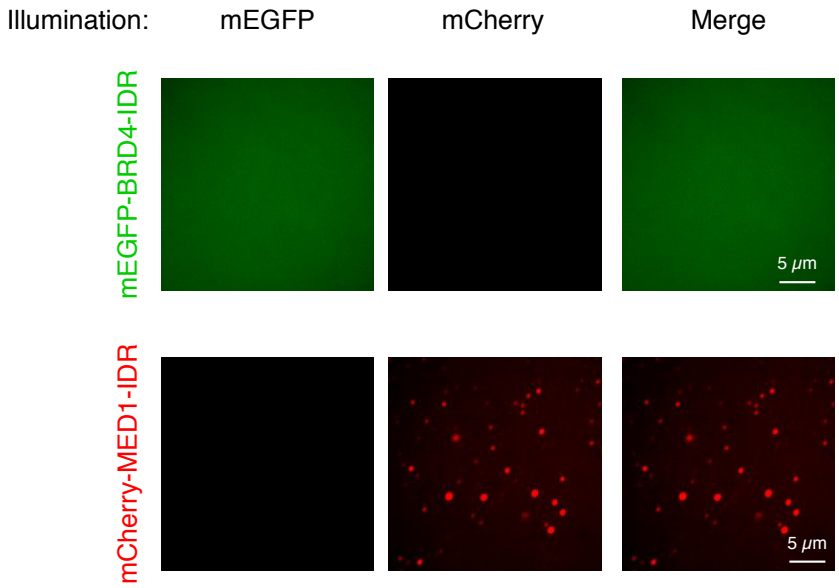

Fig. S9. BRD4-IDR does not form droplets in 10% Ficoll-400.
The indicated mEGFP or mCherry fusion proteins were mixed at 10μM each in droplet buffer containing 10% Ficoll-400 and 125mM NaCl. Individual fluorescence channels are presented, 488nm (left), 561nm (middle) and the merge of the two channels (right).

Fig. S10

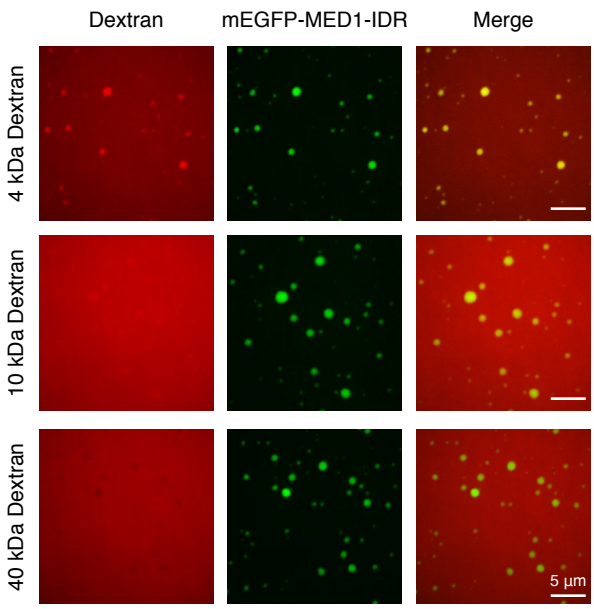

Fig. S10. Apparent mesh size of MED1-IDR droplets
MED1-IDR droplets exclude 40kDa dextrans. mEGFP-MED1-IDR droplets (10uM protein, 125mM NaCl, 10% Ficoll-400) were incubated with fluorescently labeled dextrans of the indicated average molecular weight. Representative images are presented Individual fluorescence channels are presented, 488nm (left), 561nm (middle) and the merge of the two channels (right).

Table S1.
Number of mEGFP-BRD4 or mEGFP-MED1 puncta per nucleus

	mEGFP-BRD4 puncta per nucleus
1	689
2	1483
3	1662
4	724
5	1301
6	735
7	1534
8	874
9	703
10	634
Mean:	1033.87
SEM:	129.82

	mEGFP-MED1 puncta per nucleus
1	787
2	819
3	731
4	1310
5	1102
6	815
7	1754
8	884
9	775
10	851
Mean:	982.81
SEM:	102.41

Table S2. (separate file)
Stitched enhancers in mESCs

Table S3. (separate file)
Sequence of RNA FISH probes

References and Notes

1. A. A. Hyman, C. A. Weber, F. Jülicher, Liquid-liquid phase separation in biology. *Annu. Rev. Cell Dev. Biol.* **30**, 39–58 (2014). doi:10.1146/annurev-cellbio-100913-013325 Medline

2. S. F. Banani, H. O. Lee, A. A. Hyman, M. K. Rosen, Biomolecular condensates: Organizers of cellular biochemistry. *Nat. Rev. Mol. Cell Biol.* **18**, 285–298 (2017). doi:10.1038/nrm.2017.7 Medline

3. Y. Shin, C. P. Brangwynne, Liquid phase condensation in cell physiology and disease. *Science* **357**, eaaf4382 (2017). doi:10.1126/science.aaf4382 Medline

4. C. P. Brangwynne, C. R. Eckmann, D. S. Courson, A. Rybarska, C. Hoege, J. Gharakhani, F. Jülicher, A. A. Hyman, Germline P granules are liquid droplets that localize by controlled dissolution/condensation. *Science* **324**, 1729–1732 (2009). doi:10.1126/science.1172046 Medline

5. M. Kato, T. W. Han, S. Xie, K. Shi, X. Du, L. C. Wu, H. Mirzaei, E. J. Goldsmith, J. Longgood, J. Pei, N. V. Grishin, D. E. Frantz, J. W. Schneider, S. Chen, L. Li, M. R. Sawaya, D. Eisenberg, R. Tycko, S. L. McKnight, Cell-free formation of RNA granules: Low complexity sequence domains form dynamic fibers within hydrogels. *Cell* **149**, 753–767 (2012). doi:10.1016/j.cell.2012.04.017 Medline

6. P. Li, S. Banjade, H.-C. Cheng, S. Kim, B. Chen, L. Guo, M. Llaguno, J. V. Hollingsworth, D. S. King, S. F. Banani, P. S. Russo, Q.-X. Jiang, B. T. Nixon, M. K. Rosen, Phase transitions in the assembly of multivalent signalling proteins. *Nature* **483**, 336–340 (2012). doi:10.1038/nature10879 Medline

7. Y. Lin, D. S. W. Protter, M. K. Rosen, R. Parker, Formation and Maturation of Phase-Separated Liquid Droplets by RNA-Binding Proteins. *Mol. Cell* **60**, 208–219 (2015). doi:10.1016/j.molcel.2015.08.018 Medline

8. K. Adelman, J. T. Lis, Promoter-proximal pausing of RNA polymerase II: Emerging roles in metazoans. *Nat. Rev. Genet.* **13**, 720–731 (2012). doi:10.1038/nrg3293 Medline

9. M. Bulger, M. Groudine, Functional and mechanistic diversity of distal transcription enhancers. *Cell* **144**, 327–339 (2011). doi:10.1016/j.cell.2011.01.024 Medline

10. E. Calo, J. Wysocka, Modification of enhancer chromatin: What, how, and why? *Mol. Cell* **49**, 825–837 (2013). doi:10.1016/j.molcel.2013.01.038 Medline

11. F. Spitz, E. E. M. Furlong, Transcription factors: From enhancer binding to developmental control. *Nat. Rev. Genet.* **13**, 613–626 (2012). doi:10.1038/nrg3207 Medline

12. W. Xie, B. Ren, Developmental biology. Enhancing pluripotency and lineage specification. *Science* **341**, 245–247 (2013). doi:10.1126/science.1236254 Medline

13. M. Levine, C. Cattoglio, R. Tjian, Looping back to leap forward: Transcription enters a new era. *Cell* **157**, 13–25 (2014). doi:10.1016/j.cell.2014.02.009 Medline

14. W. A. Whyte, D. A. Orlando, D. Hnisz, B. J. Abraham, C. Y. Lin, M. H. Kagey, P. B. Rahl, T. I. Lee, R. A. Young, Master transcription factors and mediator establish super-enhancers at key cell identity genes. *Cell* **153**, 307–319 (2013). doi:10.1016/j.cell.2013.03.035 Medline

15. D. Hnisz, B. J. Abraham, T. I. Lee, A. Lau, V. Saint-André, A. A. Sigova, H. A. Hoke, R. A. Young, Super-enhancers in the control of cell identity and disease. *Cell* **155**, 934–947 (2013). doi:10.1016/j.cell.2013.09.053 Medline

16. J. M. Dowen, Z. P. Fan, D. Hnisz, G. Ren, B. J. Abraham, L. N. Zhang, A. S. Weintraub, J. Schujiers, T. I. Lee, K. Zhao, R. A. Young, Control of cell identity genes occurs in insulated neighborhoods in mammalian chromosomes. *Cell* **159**, 374–387 (2014). doi:10.1016/j.cell.2014.09.030 Medline

17. D. Hnisz, A. S. Weintraub, D. S. Day, A.-L. Valton, R. O. Bak, C. H. Li, J. Goldmann, B. R. Lajoie, Z. P. Fan, A. A. Sigova, J. Reddy, D. Borges-Rivera, T. I. Lee, R. Jaenisch, M. H. Porteus, J. Dekker, R. A. Young, Activation of proto-oncogenes by disruption of chromosome neighborhoods. *Science* **351**, 1454–1458 (2016). doi:10.1126/science.aad9024 Medline

18. X. Ji, D. B. Dadon, B. E. Powell, Z. P. Fan, D. Borges-Rivera, S. Shachar, A. S. Weintraub, D. Hnisz, G. Pegoraro, T. I. Lee, T. Misteli, R. Jaenisch, R. A. Young, 3D Chromosome Regulatory Landscape of Human Pluripotent Cells. *Cell Stem Cell* **18**, 262–275 (2016). doi:10.1016/j.stem.2015.11.007 Medline

19. M. R. Mansour, B. J. Abraham, L. Anders, A. Berezovskaya, A. Gutierrez, A. D. Durbin, J. Etchin, L. Lawton, S. E. Sallan, L. B. Silverman, M. L. Loh, S. P. Hunger, T. Sanda, R. A. Young, A. T. Look, An oncogenic super-enhancer formed through somatic mutation of a noncoding intergenic element. *Science* **346**, 1373–1377 (2014). doi:10.1126/science.1259037 Medline

20. J. D. Brown, C. Y. Lin, Q. Duan, G. Griffin, A. Federation, R. M. Paranal, S. Bair, G. Newton, A. Lichtman, A. Kung, T. Yang, H. Wang, F. W. Luscinskas, K. Croce, J. E. Bradner, J. Plutzky, NF-κB directs dynamic super enhancer formation in inflammation and atherogenesis. *Mol. Cell* **56**, 219–231 (2014). doi:10.1016/j.molcel.2014.08.024 Medline

21. B. Chapuy, M. R. McKeown, C. Y. Lin, S. Monti, M. G. M. Roemer, J. Qi, P. B. Rahl, H. H. Sun, K. T. Yeda, J. G. Doench, E. Reichert, A. L. Kung, S. J. Rodig, R. A. Young, M. A. Shipp, J. E. Bradner, Discovery and characterization of super-enhancer-associated dependencies in diffuse large B cell lymphoma. *Cancer Cell* **24**, 777–790 (2013). doi:10.1016/j.ccr.2013.11.003 Medline

22. J. Lovén, H. A. Hoke, C. Y. Lin, A. Lau, D. A. Orlando, C. R. Vakoc, J. E. Bradner, T. I. Lee, R. A. Young, Selective inhibition of tumor oncogenes by disruption of super-enhancers. *Cell* **153**, 320–334 (2013). doi:10.1016/j.cell.2013.03.036 Medline

23. E. Chipumuro, E. Marco, C. L. Christensen, N. Kwiatkowski, T. Zhang, C. M. Hatheway, B. J. Abraham, B. Sharma, C. Yeung, A. Altabef, A. Perez-Atayde, K.-K. Wong, G.-C. Yuan, N. S. Gray, R. A. Young, R. E. George, CDK7 inhibition suppresses super-enhancer-linked oncogenic transcription in MYCN-driven cancer. *Cell* **159**, 1126–1139 (2014). doi:10.1016/j.cell.2014.10.024 Medline

24. N. Kwiatkowski, T. Zhang, P. B. Rahl, B. J. Abraham, J. Reddy, S. B. Ficarro, A. Dastur, A. Amzallag, S. Ramaswamy, B. Tesar, C. E. Jenkins, N. M. Hannett, D. McMillin, T. Sanda, T. Sim, N. D. Kim, T. Look, C. S. Mitsiades, A. P. Weng, J. R. Brown, C. H. Benes, J. A. Marto, R. A. Young, N. S. Gray, Targeting transcription regulation in cancer

with a covalent CDK7 inhibitor. *Nature* **511**, 616–620 (2014). doi:10.1038/nature13393 Medline

25. Y. Wang, T. Zhang, N. Kwiatkowski, B. J. Abraham, T. I. Lee, S. Xie, H. Yuzugullu, T. Von, H. Li, Z. Lin, D. G. Stover, E. Lim, Z. C. Wang, J. D. Iglehart, R. A. Young, N. S. Gray, J. J. Zhao, CDK7-dependent transcriptional addiction in triple-negative breast cancer. *Cell* **163**, 174–186 (2015). doi:10.1016/j.cell.2015.08.063 Medline

26. D. Hnisz, J. Schuijers, C. Y. Lin, A. S. Weintraub, B. J. Abraham, T. I. Lee, J. E. Bradner, R. A. Young, Convergence of developmental and oncogenic signaling pathways at transcriptional super-enhancers. *Mol. Cell* **58**, 362–370 (2015). doi:10.1016/j.molcel.2015.02.014 Medline

27. T. Jiang, R. Raviram, V. Snetkova, P. P. Rocha, C. Proudhon, S. Badri, R. Bonneau, J. A. Skok, Y. Kluger, Identification of multi-loci hubs from 4C-seq demonstrates the functional importance of simultaneous interactions. *Nucleic Acids Res.* **44**, 8714–8725 (2016). doi:10.1093/nar/gkw568 Medline

28. C. Proudhon, V. Snetkova, R. Raviram, C. Lobry, S. Badri, T. Jiang, B. Hao, T. Trimarchi, Y. Kluger, I. Aifantis, R. Bonneau, J. A. Skok, Active and Inactive Enhancers Cooperate to Exert Localized and Long-Range Control of Gene Regulation. *Cell Rep.* **15**, 2159–2169 (2016). Medline

29. H. Y. Shin, M. Willi, K. HyunYoo, X. Zeng, C. Wang, G. Metser, L. Hennighausen, Hierarchy within the mammary STAT5-driven *Wap* super-enhancer. *Nat. Genet.* **48**, 904–911 (2016). doi:10.1038/ng.3606 Medline

30. D. Hnisz, K. Shrinivas, R. A. Young, A. K. Chakraborty, P. A. Sharp, A Phase Separation Model for Transcriptional Control. *Cell* **169**, 13–23 (2017). doi:10.1016/j.cell.2017.02.007 Medline

31. Z. Yang, J. H. N. Yik, R. Chen, N. He, M. K. Jang, K. Ozato, Q. Zhou, Recruitment of P-TEFb for stimulation of transcriptional elongation by the bromodomain protein Brd4. *Mol. Cell* **19**, 535–545 (2005). doi:10.1016/j.molcel.2005.06.029 Medline

32. M. K. Jang, K. Mochizuki, M. Zhou, H.-S. Jeong, J. N. Brady, K. Ozato, The bromodomain protein Brd4 is a positive regulatory component of P-TEFb and stimulates RNA polymerase II-dependent transcription. *Mol. Cell* **19**, 523–534 (2005). doi:10.1016/j.molcel.2005.06.027 Medline

33. R. Di Micco, B. Fontanals-Cirera, V. Low, P. Ntziachristos, S. K. Yuen, C. D. Lovell, I. Dolgalev, Y. Yonekubo, G. Zhang, E. Rusinova, G. Gerona-Navarro, M. Cañamero, M. Ohlmeyer, I. Aifantis, M. M. Zhou, A. Tsirigos, E. Hernando, Control of embryonic stem cell identity by BRD4-dependent transcriptional elongation of super-enhancer-associated pluripotency genes. *Cell Rep.* **9**, 234–247 (2014). Medline

34. J. Soutourina, S. Wydau, Y. Ambroise, C. Boschiero, M. Werner, Direct interaction of RNA polymerase II and mediator required for transcription in vivo. *Science* **331**, 1451–1454 (2011). doi:10.1126/science.1200188 Medline

35. J. Soutourina, Transcription regulation by the Mediator complex. *Nat. Rev. Mol. Cell Biol.* **19**, 262–274 (2018). Medline

36. T. J. Nott, E. Petsalaki, P. Farber, D. Jervis, E. Fussner, A. Plochowietz, T. D. Craggs, D. P. Bazett-Jones, T. Pawson, J. D. Forman-Kay, A. J. Baldwin, Phase transition of a disordered nuage protein generates environmentally responsive membraneless organelles. *Mol. Cell* **57**, 936–947 (2015). doi:10.1016/j.molcel.2015.01.013 Medline

37. C. W. Pak, M. Kosno, A. S. Holehouse, S. B. Padrick, A. Mittal, R. Ali, A. A. Yunus, D. R. Liu, R. V. Pappu, M. K. Rosen, Sequence Determinants of Intracellular Phase Separation by Complex Coacervation of a Disordered Protein. *Mol. Cell* **63**, 72–85 (2016). doi:10.1016/j.molcel.2016.05.042 Medline

38. C. P. Brangwynne, T. J. Mitchison, A. A. Hyman, Active liquid-like behavior of nucleoli determines their size and shape in Xenopus laevis oocytes. *Proc. Natl. Acad. Sci. U.S.A.* **108**, 4334–4339 (2011). doi:10.1073/pnas.1017150108 Medline

39. A. Patel, L. Malinovska, S. Saha, J. Wang, S. Alberti, Y. Krishnan, A. A. Hyman, ATP as a biological hydrotrope. *Science* **356**, 753–756 (2017). doi:10.1126/science.aaf6846 Medline

40. S. Kroschwald, S. Maharana, A. Simon, Hexanediol: A chemical probe to investigate the material properties of membrane-less compartments. *Matters* 10.19185/matters.201702000010 (2017).

41. C. Y. Lin, J. Lovén, P. B. Rahl, R. M. Paranal, C. B. Burge, J. E. Bradner, T. I. Lee, R. A. Young, Transcriptional amplification in tumor cells with elevated c-Myc. *Cell* **151**, 56–67 (2012). doi:10.1016/j.cell.2012.08.026 Medline

42. S. Elbaum-Garfinkle, Y. Kim, K. Szczepaniak, C. C.-H. Chen, C. R. Eckmann, S. Myong, C. P. Brangwynne, The disordered P granule protein LAF-1 drives phase separation into droplets with tunable viscosity and dynamics. *Proc. Natl. Acad. Sci. U.S.A.* **112**, 7189–7194 (2015). doi:10.1073/pnas.1504822112 Medline

43. C. P. Brangwynne, Phase transitions and size scaling of membrane-less organelles. *J. Cell Biol.* **203**, 875–881 (2013). doi:10.1083/jcb.201308087 Medline

44. Y. Shin, J. Berry, N. Pannucci, M. P. Haataja, J. E. Toettcher, C. P. Brangwynne, Spatiotemporal Control of Intracellular Phase Transitions Using Light-Activated optoDroplets. *Cell* **168**, 159–171.e14 (2017). doi:10.1016/j.cell.2016.11.054 Medline

45. I. Ozkan-Dagliyan, Y.-Y. Chiou, R. Ye, B. H. Hassan, N. Ozturk, A. Sancar, Formation of Arabidopsis Cryptochrome 2 photobodies in mammalian nuclei: Application as an optogenetic DNA damage checkpoint switch. *J. Biol. Chem.* **288**, 23244–23251 (2013). doi:10.1074/jbc.M113.493361 Medline

46. X. Yu, R. Sayegh, M. Maymon, K. Warpeha, J. Klejnot, H. Yang, J. Huang, J. Lee, L. Kaufman, C. Lin, Formation of nuclear bodies of Arabidopsis CRY2 in response to blue light is associated with its blue light-dependent degradation. *Plant Cell* **21**, 118–130 (2009). doi:10.1105/tpc.108.061663 Medline

47. M.-T. Wei, S. Elbaum-Garfinkle, A. S. Holehouse, C. C.-H. Chen, M. Feric, C. B. Arnold, R. D. Priestley, R. V. Pappu, C. P. Brangwynne, Phase behaviour of disordered proteins underlying low density and high permeability of liquid organelles. *Nat. Chem.* **9**, 1118–1125 (2017). doi:10.1038/nchem.2803 Medline

48. H. I. Suzuki, R. A. Young, P. A. Sharp, Super-Enhancer-Mediated RNA Processing Revealed by Integrative MicroRNA Network Analysis. *Cell* **168**, 1000–1014.e15 (2017). doi:10.1016/j.cell.2017.02.015 Medline

49. J. E. Bradner, D. Hnisz, R. A. Young, Transcriptional Addiction in Cancer. *Cell* **168**, 629–643 (2017). doi:10.1016/j.cell.2016.12.013 Medline

50. M. Ptashne, How eukaryotic transcriptional activators work. *Nature* **335**, 683–689 (1988). doi:10.1038/335683a0 Medline

51. P. J. Mitchell, R. Tjian, Transcriptional regulation in mammalian cells by sequence-specific DNA binding proteins. *Science* **245**, 371–378 (1989). doi:10.1126/science.2667136 Medline

52. J. Liu, N. B. Perumal, C. J. Oldfield, E. W. Su, V. N. Uversky, A. K. Dunker, Intrinsic disorder in transcription factors. *Biochemistry* **45**, 6873–6888 (2006). doi:10.1021/bi0602718 Medline

53. H. Xie, S. Vucetic, L. M. Iakoucheva, C. J. Oldfield, A. K. Dunker, V. N. Uversky, Z. Obradovic, Functional anthology of intrinsic disorder. 1. Biological processes and functions of proteins with long disordered regions. *J. Proteome Res.* **6**, 1882–1898 (2007). doi:10.1021/pr060392u Medline

54. S. F. Banani, A. M. Rice, W. B. Peeples, Y. Lin, S. Jain, R. Parker, M. K. Rosen, Compositional Control of Phase-Separated Cellular Bodies. *Cell* **166**, 651–663 (2016). doi:10.1016/j.cell.2016.06.010 Medline

55. R. A. Beagrie, A. Scialdone, M. Schueler, D. C. Kraemer, M. Chotalia, S. Q. Xie, M. Barbieri, I. de Santiago, L. M. Lavitas, M. R. Branco, J. Fraser, J. Dostie, L. Game, N. Dillon, P. A. Edwards, M. Nicodemi, A. Pombo, Complex multi-enhancer contacts captured by genome architecture mapping. *Nature* **543**, 519–524 (2017). Medline

56. S. S. P. Rao, S.-C. Huang, B. Glenn St Hilaire, J. M. Engreitz, E. M. Perez, K.-R. Kieffer-Kwon, A. L. Sanborn, S. E. Johnstone, G. D. Bascom, I. D. Bochkov, X. Huang, M. S. Shamim, J. Shin, D. Turner, Z. Ye, A. D. Omer, J. T. Robinson, T. Schlick, B. E. Bernstein, R. Casellas, E. S. Lander, E. L. Aiden, Cohesin Loss Eliminates All Loop Domains. *Cell* **171**, 305–320.e24 (2017). doi:10.1016/j.cell.2017.09.026 Medline

57. W.-K. Cho, J.-H. Spille, M. Hecht, C. Lee, C. Li, V. Grube, I. I. Cisse, Mediator and RNA polymerase II clusters associate in transcription-dependent condensates. *Science* 10.1126/science.aar4199 (2018).

58. W.-K. Cho, N. Jayanth, B. P. English, T. Inoue, J. O. Andrews, W. Conway, J. B. Grimm, J.-H. Spille, L. D. Lavis, T. Lionnet, I. I. Cisse, RNA Polymerase II cluster dynamics predict mRNA output in living cells. *eLife* **5**, 1123 (2016). doi:10.7554/eLife.13617 Medline

59. A. G. Larson, D. Elnatan, M. M. Keenen, M. J. Trnka, J. B. Johnston, A. L. Burlingame, D. A. Agard, S. Redding, G. J. Narlikar, Liquid droplet formation by HP1α suggests a role for phase separation in heterochromatin. *Nature* **547**, 236–240 (2017). doi:10.1038/nature22822 Medline

60. A. R. Strom, A. V. Emelyanov, M. Mir, D. V. Fyodorov, X. Darzacq, G. H. Karpen, Phase separation drives heterochromatin domain formation. *Nature* **547**, 241–245 (2017). doi:10.1038/nature22989 Medline

61. M. Feric, N. Vaidya, T. S. Harmon, D. M. Mitrea, L. Zhu, T. M. Richardson, R. W. Kriwacki, R. V. Pappu, C. P. Brangwynne, Coexisting Liquid Phases Underlie Nucleolar Subcompartments. *Cell* **165**, 1686–1697 (2016). doi:10.1016/j.cell.2016.04.047 Medline

62. T. S. Harmon, A. S. Holehouse, M. K. Rosen, R. V. Pappu, Intrinsically disordered linkers determine the interplay between phase separation and gelation in multivalent proteins. *eLife* **6**, e30294 (2017). doi:10.7554/eLife.30294 Medline

63. J. A. Riback, C. D. Katanski, J. L. Kear-Scott, E. V. Pilipenko, A. E. Rojek, T. R. Sosnick, D. A. Drummond, Stress-Triggered Phase Separation Is an Adaptive, Evolutionarily Tuned Response. *Cell* **168**, 1028–1040.e19 (2017). doi:10.1016/j.cell.2017.02.027 Medline

64. S. Boeynaems, E. Bogaert, D. Kovacs, A. Konijnenberg, E. Timmerman, A. Volkov, M. Guharoy, M. De Decker, T. Jaspers, V. H. Ryan, A. M. Janke, P. Baatsen, T. Vercruysse, R.-M. Kolaitis, D. Daelemans, J. P. Taylor, N. Kedersha, P. Anderson, F. Impens, F. Sobott, J. Schymkowitz, F. Rousseau, N. L. Fawzi, W. Robberecht, P. Van Damme, P. Tompa, L. Van Den Bosch, Phase Separation of C9orf72 Dipeptide Repeats Perturbs Stress Granule Dynamics. *Mol. Cell* **65**, 1044–1055.e5 (2017). doi:10.1016/j.molcel.2017.02.013 Medline

65. J. P. Brady, P. J. Farber, A. Sekhar, Y.-H. Lin, R. Huang, A. Bah, T. J. Nott, H. S. Chan, A. J. Baldwin, J. D. Forman-Kay, L. E. Kay, Structural and hydrodynamic properties of an intrinsically disordered region of a germ cell-specific protein on phase separation. *Proc. Natl. Acad. Sci. U.S.A.* **114**, E8194–E8203 (2017). doi:10.1073/pnas.1706197114 Medline

66. A. Patel, H. O. Lee, L. Jawerth, S. Maharana, M. Jahnel, M. Y. Hein, S. Stoynov, J. Mahamid, S. Saha, T. M. Franzmann, A. Pozniakovski, I. Poser, N. Maghelli, L. A. Royer, M. Weigert, E. W. Myers, S. Grill, D. Drechsel, A. A. Hyman, S. Alberti, A Liquid-to-Solid Phase Transition of the ALS Protein FUS Accelerated by Disease Mutation. *Cell* **162**, 1066–1077 (2015). doi:10.1016/j.cell.2015.07.047 Medline

67. A. Molliex, J. Temirov, J. Lee, M. Coughlin, A. P. Kanagaraj, H. J. Kim, T. Mittag, J. P. Taylor, Phase separation by low complexity domains promotes stress granule assembly and drives pathological fibrillization. *Cell* **163**, 123–133 (2015). doi:10.1016/j.cell.2015.09.015 Medline

68. A. Jain, R. D. Vale, RNA phase transitions in repeat expansion disorders. *Nature* **546**, 243–247 (2017). Medline

69. S. Malik, R. G. Roeder, in *Nuclear Receptors*, vol. 364 of *Methods in Enzymology* (Elsevier, 2003), pp. 257–284.

70. S. Albini, P. Coutinho Toto, A. Dall'Agnese, B. Malecova, C. Cenciarelli, A. Felsani, M. Caruso, S. J. Bultman, P. L. Puri, Brahma is required for cell cycle arrest and late muscle gene expression during skeletal myogenesis. *EMBO Rep.* **16**, 1037–1050 (2015). doi:10.15252/embr.201540159 Medline

71. J. Schindelin, I. Arganda-Carreras, E. Frise, V. Kaynig, M. Longair, T. Pietzsch, S. Preibisch, C. Rueden, S. Saalfeld, B. Schmid, J.-Y. Tinevez, D. J. White, V. Hartenstein, K. Eliceiri, P. Tomancak, A. Cardona, Fiji: An open-source platform for biological-image analysis. *Nat. Methods* **9**, 676–682 (2012). doi:10.1038/nmeth.2019 Medline

72. A. Baddeley, E. Rubak, R. Turner, *Spatial Point Patterns: Methodology and Applications with R* (Chapman and Hall/CRC Press, 2015).

73. B. L. Sprague, R. L. Pego, D. A. Stavreva, J. G. McNally, Analysis of binding reactions by fluorescence recovery after photobleaching. *Biophys. J.* **86**, 3473–3495 (2004). doi:10.1529/biophysj.103.026765 Medline

74. D. Mazza, A. Abernathy, N. Golob, T. Morisaki, J. G. McNally, A benchmark for chromatin binding measurements in live cells. *Nucleic Acids Res.* **40**, e119 (2012). doi:10.1093/nar/gks701 Medline

75. C. Trapnell, L. Pachter, S. L. Salzberg, TopHat: Discovering splice junctions with RNA-Seq. *Bioinformatics* **25**, 1105–1111 (2009). doi:10.1093/bioinformatics/btp120 Medline

76. L. Wang, S. Wang, W. Li, RSeQC: Quality control of RNA-seq experiments. *Bioinformatics* **28**, 2184–2185 (2012). doi:10.1093/bioinformatics/bts356 Medline

77. B. Langmead, C. Trapnell, M. Pop, S. L. Salzberg, Ultrafast and memory-efficient alignment of short DNA sequences to the human genome. *Genome Biol.* **10**, R25 (2009). doi:10.1186/gb-2009-10-3-r25 Medline

78. Y. Zhang, T. Liu, C. A. Meyer, J. Eeckhoute, D. S. Johnson, B. E. Bernstein, C. Nusbaum, R. M. Myers, M. Brown, W. Li, X. S. Liu, Model-based analysis of ChIP-Seq (MACS). *Genome Biol.* **9**, R137 (2008). doi:10.1186/gb-2008-9-9-r137 Medline

79. W. J. Kent, C. W. Sugnet, T. S. Furey, K. M. Roskin, T. H. Pringle, A. M. Zahler, D. Haussler, The human genome browser at UCSC. *Genome Res.* **12**, 996–1006 (2002). doi:10.1101/gr.229102 Medline

80. A. R. Quinlan, I. M. Hall, BEDTools: A flexible suite of utilities for comparing genomic features. *Bioinformatics* **26**, 841–842 (2010). doi:10.1093/bioinformatics/btq033 Medline

81. H. Li, B. Handsaker, A. Wysoker, T. Fennell, J. Ruan, N. Homer, G. Marth, G. Abecasis, R. Durbin, 1000 Genome Project Data Processing Subgroup, The Sequence Alignment/Map format and SAMtools. *Bioinformatics* **25**, 2078–2079 (2009). doi:10.1093/bioinformatics/btp352 Medline

82. V. K. Mootha, C. M. Lindgren, K.-F. Eriksson, A. Subramanian, S. Sihag, J. Lehar, P. Puigserver, E. Carlsson, M. Ridderstråle, E. Laurila, N. Houstis, M. J. Daly, N. Patterson, J. P. Mesirov, T. R. Golub, P. Tamayo, B. Spiegelman, E. S. Lander, J. N. Hirschhorn, D. Altshuler, L. C. Groop, PGC-1alpha-responsive genes involved in oxidative phosphorylation are coordinately downregulated in human diabetes. *Nat. Genet.* **34**, 267–273 (2003). doi:10.1038/ng1180 Medline